

Transworld Research Network  
37/661 (2), Fort P.O., Trivandrum-695 023, Kerala, India



Recent Res. Dev. Chem. Physics, 5(2004): ISBN: 81-7895-155-X

## Coherent laser spectroscopy of transient molecules and free radicals

Ju Xin<sup>1</sup>, Ionela Ionescu<sup>2</sup>, Haiyan Fan<sup>2</sup> and Scott A. Reid<sup>2</sup>

<sup>1</sup>Department of Physics and Engineering Technologies, Bloomsburg University, Bloomsburg PA 17815, USA; <sup>2</sup>Department of Chemistry, Marquette University, Milwaukee, WI 53201 USA

### Abstract

*Recent years have witnessed great advances in the study of molecular spectroscopy and dynamics using coherent laser spectroscopy. In this article, we review recent work from our laboratory concerning the application of coherent laser techniques such as polarization quantum beat spectroscopy and transient laser induced grating spectroscopy to the study of transient molecules and free radicals. Highlighted systems include CN, OH and OD, NO<sub>2</sub>, and HCF.*

### I. Introduction

In recent years, the coherent properties of matter-radiation interactions have been increasingly exploited for the study of molecular spectroscopy and dynamics [1-10]. While many diverse methodologies have been developed, exploiting both resonant and non-resonant interactions, a typical feature of single-molecule

phenomena is the creation of molecular superposition states via coherent laser excitation. The time evolution of the prepared superposition yields (by Fourier transformation) information on the energy levels of the chromophore and dephasing processes in the excited state, at a resolution limited by the uncertainty principle. In some cases, the resolution is far superior to that obtainable by frequency domain methods [5-7].

A particularly exciting application of coherent laser techniques is to the detection, spectroscopy, and dynamics of transient molecules and free radicals[3,11-24], which are important in a variety of chemical environments including combustion, atmospheric chemistry, and interstellar chemistry. Recent years have witnessed a tremendous growth in our knowledge of the chemistry and spectroscopy of transient species[8,21]. In this article, we will illustrate the application of coherent laser spectroscopic techniques to a variety of transient molecules and free radicals, including CN, NO<sub>2</sub>, OH/OD, and HCF. The work presented will focus on the application of polarization quantum beat spectroscopy to probe hyperfine interactions and Zeeman effects in excited electronic states of these species, yielding detailed information on their electronic structure.

The outline of the article is as follows. Section II provides a background on coherent laser techniques and quantum beat spectroscopy. Section III discusses experimental considerations in the application of coherent techniques to transient molecules and free radicals, including methods for generating these species and data acquisition procedures. Section IV presents recent experimental results from our laboratory that highlight the utility of coherent laser techniques for probing transient molecules and open-shell species, while Section V gives a summary and conclusion.

## II. Coherent laser spectroscopy: Background

The general requirement for coherent laser spectroscopy is that the coherence width of the source should encompass the manifold of states to be examined (i.e.,  $\Gamma > \Delta E$ , where  $\Delta E$  is the spacing of the eigenstates). For the  $\sim 5$  ns pulse duration characteristic of Nd:YAG pumped dye laser systems, the coherence width is  $\sim 100$  MHz, and interrogation is limited to molecular fine and hyperfine structure. Considering a manifold of excited states  $|e\rangle$ , a typical experiment will involve excitation, or preparation of coherences among the set of states  $|e\rangle$ , and detection, or probing the subsequent time evolution. A schematic of this arrangement for a simple four level system is shown in Figure 1, which displays several possible detection schemes.

The most convenient and simplest to implement of the schemes shown in Fig. 1 is detection of fluorescence to lower lying states[5-7], which is the primary method employed in our work. However, in comparison with state-selected detection, this method suffers from a reduced modulation depth due to incoherent contributions from emission to (typically) several final states. As an illustration, Figure 2 displays waveforms for the  $R(0)$  transition of a vibronic band near 488 nm in NO<sub>2</sub> obtained using fluorescence detected quantum beat spectroscopy (upper panel) and laser induced grating spectroscopy (lower panel), which provides state-selected detection [23]. The coherences reflect interferences among coherently excited hyperfine levels, and the greater contrast in the latter is evident, as well as a much shorter overall decay time due to washout of the induced grating via molecular motion in the jet [23].

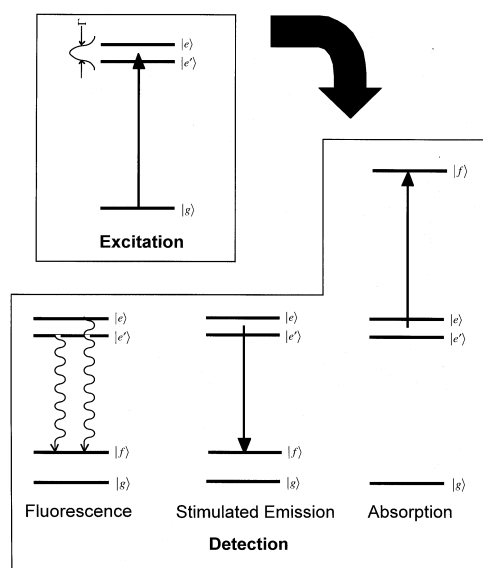


**Figure 1.** Illustration of coherent laser spectroscopy. Excitation prepares a coherent superposition of the molecular eigenstates  $|e\rangle$  and  $|e'\rangle$ , and the subsequent time evolution can be detected in a variety of ways, as illustrated.

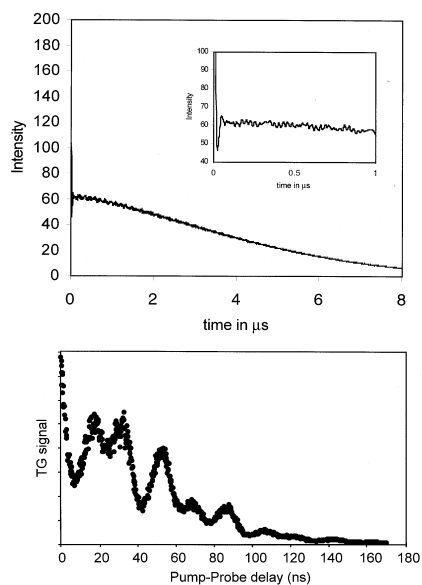


**Figure 2.** Comparison of quantum beats for an R(0) line in an  $\text{NO}_2$  band near 488 nm detected using fluorescence (upper panel) and laser-induced grating spectroscopy (lower panel).

The observable manifestations of time evolution depend sensitively on the quantum numbers of the set  $|e\rangle$ . As an example, using the four level system described in figure 1, coherences among levels  $|e\rangle$  and  $|e'\rangle$  with the same total angular momentum will give rise to modulated *isotropic* fluorescence emission. For polyatomic molecules, such beats were first observed by McDonald and co-workers in the  $S_1$  states of biacetyl and methyglyoxal[25,26], where they arise from singlet-triplet interactions. Huber and co-workers have conducted extensive studies of isotropic quantum beats in the  $S_1$  state of propynal[27-29], and shown that Zeeman quantum beats can be observed under the selection rule  $\Delta M = 0$ , which allows the magnitude (but not sign) of the Landé  $g$ -factors to be determined[28].

In contrast to isotropic quantum beats, coherences among levels  $|e\rangle$  and  $|e'\rangle$  with different total angular momentum give rise to *anisotropic* quantum beats, which require polarization specific detection and disappear for unpolarized detection[5]. At zero-field, polarization quantum beats can be observed between different hyperfine ( $F$ ) components of a molecular state, providing valuable information on the interactions of electron and nuclear spins with molecular rotation. We illustrate the case of hyperfine polarization quantum beats using the  $\tilde{A}^1A''$  state of HCF, where the coupling scheme:  $\mathbf{F}_1 = \mathbf{J} + \mathbf{I}_F$ ,  $\mathbf{F} = \mathbf{F}_1 + \mathbf{I}_H$  is employed. Using the density matrix formalism of Blum[30], and assuming that the hyperfine interaction is sufficiently weak so that  $J$  remains a good quantum number, the time dependent perturbation coefficient which reflects the time dependence of the state multipoles is given by[30]:

$$G(t)_K^H = \frac{1}{(2I_F + 1)(2I_H + 1)} \sum_{\substack{F_1', F_1 \\ F', F}} (2F_1 + 1)(2F_1' + 1)(2F + 1)(2F' + 1) \\ \times \begin{Bmatrix} F_1' & F_1' & I_H \\ F & F_1 & K \end{Bmatrix}^2 \begin{Bmatrix} J & F_1' & I_F \\ F_1 & J & K \end{Bmatrix}^2 \\ \times e^{-\left[ i(E_{F', F_1'} - E_{F, F_1})t/\hbar - (\gamma_{F', F_1'} + \gamma_{F, F_1})t/2 \right]} \quad (1)$$

In equation (1) the summation runs over all hyperfine levels, and it is assumed that the nuclear spins are unaffected by excitation and decay processes[30]. Figure 3 displays a comparison of experimental and calculated quantum beat spectra for the  $rR(0)$  line in the (0,2,1) level of the  $\tilde{A}^1A''$  state of HCF, where the calculated spectrum was obtained by Fourier Transform of the time dependence represented by equation (1).

Polarization quantum beats can also be observed between Zeeman and Stark split molecular states, under a selection rule  $\Delta M = \pm 2$  for appropriate choice of excitation and detection polarizations[31,32]. In contrast to the isotropic case, polarization Zeeman quantum beat spectroscopy can be used to determine the sign of the Landé  $g$ -factors[13,30-32]. In addition, very small  $g$ -factors can be measured due to the intrinsically high resolution of QBS. For example, in the  $\tilde{A}^1A''$  state of HCF we have measured  $g$ -factors of  $\sim 0.03$  to a precision of  $\sim 2\%$  using magnetic fields of only  $\sim 30$  G.

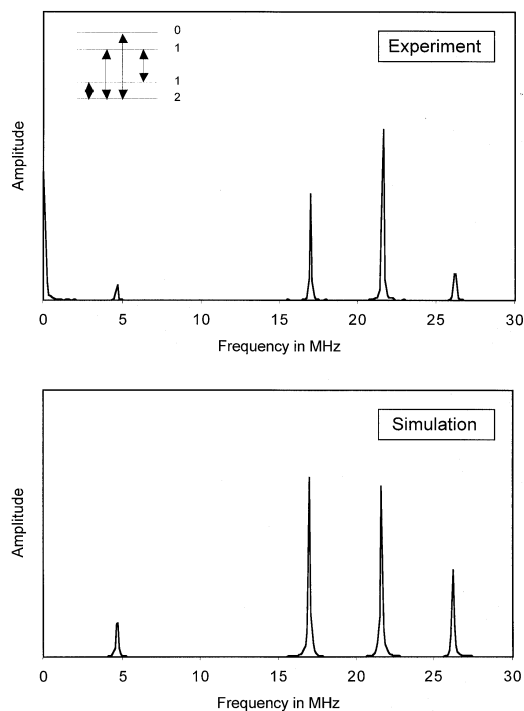


**Figure 3.** Comparison of experimental (upper panel) and calculated (lower panel) polarization quantum beat spectra for the  $rR(\theta)$  line in the  $(0, 2, 1)$  level of the  $\tilde{A}^1A''$  state of HCF. The calculated spectrum was obtained as described in the text.

An expression for the intensity of the time resolved emission in the case of polarization quantum beats includes a modulated anisotropic component of the form[5-7]:

$$\sum_i A_i \cos(\omega_i t) P_2(\cos \theta), \quad (2)$$

where the index  $i$  labels each quantum beat, and  $\theta$  is the angle between (linear) excitation and detection polarizations. Comparing the special cases of  $\theta = 0^\circ$  and  $90^\circ$ , eq. (2) predicts a change in amplitude (by a factor of 2) and change in phase (by  $180^\circ$ ) of the beats. Panel (a) of Figure 4 illustrates this for Zeeman polarization quantum beats in the  $v = 0, N = 1, J = 3/2$  level of the  $\tilde{B}^2 \Sigma^+$  state of the CN radical.

### III. Coherent laser spectroscopy: Experimental considerations

#### A. Production of transient molecules and free radicals

Typically, our studies of transient molecules and free radicals have employed a pulsed discharge source, which is well matched with species-specific methods of

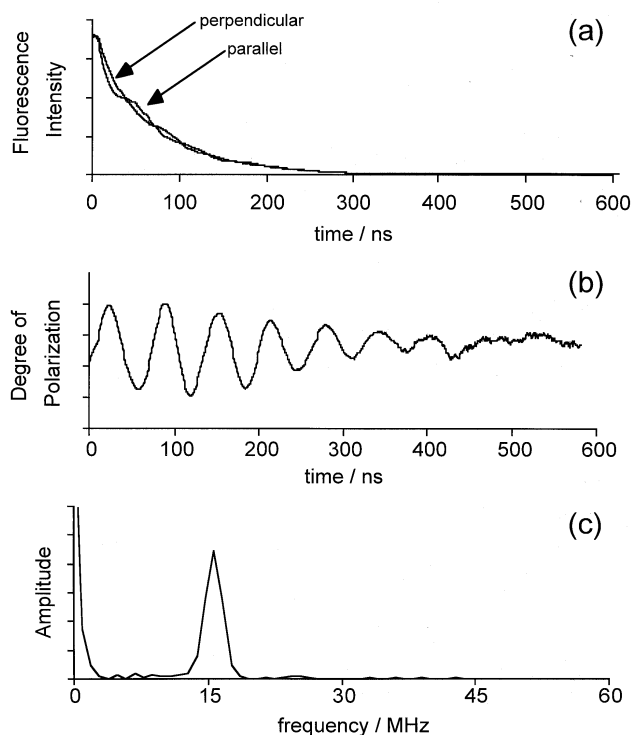


**Figure 4.** Zeeman polarization quantum beats in the  $\nu = 0, N = 1, J = 3/2$  level of the  $\tilde{B}^2 \Sigma^+$  state of the CN radical. Panel (a) : Fluorescence waveforms collected for parallel and perpendicular laser-detector polarizations at a magnetic field of 13.9 G. Panel (b) : Time dependent degree of polarization, calculated as described in the text. Panel (c) : Fourier transform of the time-dependent degree of polarization.

detection such as laser induced fluorescence (LIF). The nozzle has previously been described in detail[33], and is similar to other designs in the literature[17,19]. Typically, a pulsed electrical discharge (800-1200 V pulse, 10-50  $\mu$ s duration, < 1 mA current) is initiated through a  $\sim$  2% mixture of precursor seeded in Argon that was premixed in a stainless steel cylinder. The typical backing pressure was  $\sim$  1 bar, and the gas pulse typically of  $\sim$  1 ms duration. The timing of laser, nozzle, and discharge is controlled via a digital delay generator (SRS DG-535). The laser system consists of an etalon narrowed dye laser (Lambda-Physik Scanmate 2E), pumped by the second or third harmonic of an injection seeded Nd:YAG laser (Continuum Powerlite 7010 or NY61). The laser beam was not focused, and typical pulse energies were  $\sim$ 500  $\mu$ J in a  $\sim$  3 mm diameter beam. A quartz window was used to direct a portion of the dye laser fundamental into a Fe-Ne or Fe-Ar hollow cathode lamp for absolute wavelength calibration using the optogalvanic effect.

The measurements typically utilized a mutually orthogonal geometry of laser, molecular beam, and detector, where the laser beam crossed the molecular beam at  $\sim$  20

nozzle diameters downstream. Fluorescence was collected by a two lens  $f/2.4$  condenser assembly, and passed through an appropriate long-pass cutoff filter (Corion) and linear polarizer (typical extinction ratio of  $10^5$ ) prior to striking a photomultiplier tube detector held at typically  $-600$  V. The PMT output was terminated into  $50 \Omega$  and digitized by an oscilloscope (HP 54521A) at a typical sampling rate of 1 GHz and record length of 4096 points.

## B. Data collection procedure for quantum beat spectroscopy

The data collection procedure for polarization quantum beat spectroscopy is as follows. Fluorescence waveforms averaged over 2000–5000 laser shots are collected for parallel and perpendicular laser-detector polarizations, and the time-dependent degree of polarization  $[P(t)]$  is calculated via the relation:

$$P(t) = \frac{I_{\parallel}(t) - I_{\perp}(t)}{I_{\parallel}(t) + I_{\perp}(t)}. \quad (3)$$

The quantum beat spectrum is the Fourier Transform of the time-dependent degree of polarization. An example is shown Figure 4 for Zeeman polarization quantum beats in the  $v = 0, N = 1, J = 3/2$  level of the  $\tilde{B}^2 \Sigma^+$  state of the CN radical. Panel (a) displays the parallel and perpendicular waveforms at a magnetic field strength of 13.9 G, while panel (b) displays the degree of polarization calculated using equation (3). The Fourier transform of the degree of polarization is shown in the panel (c), which reveals one strong quantum beat centered around 16 MHz.

## IV. Applications of coherent laser spectroscopy to transient molecules and free radicals

### A. Probing the vibrational state dependence of hyperfine interactions and interactions for weakly bound levels: $\text{NO}_2$

The dynamics of radical-radical reactions are often influenced by long-range electrostatic interactions, and  $\text{NO}_2$  presents a rare opportunity to examine the spectroscopic manifestations of such interactions in a *chemically bound* system. The well-known complexity of the  $\text{NO}_2$  visible spectrum arises from the coupling of  $a_1$  ( $b_2$ ) vibronic levels of the  ${}^2\text{B}_2$  excited state with  $b_2$  ( $a_1$ ) levels of the ground state ( ${}^2\text{A}_1$ ), and vibronic chaos is well established at energies around  $16,500 \text{ cm}^{-1}$ [34-36]. Over the past decade, the region near  $\text{D}_0$  has been extensively studied[37-46], and it is now well-established that the density of states increases significantly in the  $15 \text{ cm}^{-1}$  region below  $\text{D}_0$ . Different mechanisms that have been proposed to account for the additional level density near  $\text{D}_0$ , including: (a) long-range electrostatic interactions[46], and (b) interactions with other electronic states which are repulsive at short-range but weakly attractive at long-range[44,45,47].

Interest in the hyperfine structure of levels near  $\text{D}_0$  was sparked by Romanini, *et al.*, who detected 2-photon transitions to levels near  $\text{D}_0$  using continuous-wave cavity ring down spectroscopy, and reported level splittings similar to the hyperfine structure of a free NO molecule[43]. We obtained the first measurement of the hyperfine structure of

levels near  $D_0$  using polarization quantum beat spectroscopy[48]. Figure 5 displays a typical hyperfine quantum beat spectrum (upper panel) for a  $J=3/2$  eigenstate near  $D_0$ , marked by an arrow in the laser induced fluorescence spectrum (lower panel). Note the abrupt cutoff in the fluorescence spectrum, which signals the onset of dissociation. Our study of  $J=3/2$  eigenstates in the region below  $D_0$  using polarization QBS did not reveal a hyperfine structure characteristic of free NO, but did show that the average hyperfine splittings were very small, around five times smaller on the average than observed at energies below  $\sim 22\,000\text{ cm}^{-1}$ [48].

We investigated the origin of the unexpectedly small hyperfine structure near  $D_0$  by probing the evolution of this structure with increasing energy[49]. In  $\text{NO}_2$ , hyperfine spectroscopy is a sensitive probe of the strong  $\tilde{X}^2A_1/\tilde{A}^2B_2$  vibronic coupling, due to the intrinsically small Fermi-contact interaction of  $\tilde{A}^2B_2$ . When combined with previous work at lower energies[50-54], our studies revealed a gradual weakening of the Fermi-contact interaction with increasing energy. A comparison with theoretical predictions for the  $16\,600\text{--}18\,700\text{ cm}^{-1}$  region indicates that the primary cause is vibrational averaging of the  $\tilde{X}^2A_1$  Fermi-contact interaction, an effect which contributes to the small hyperfine splittings observed near dissociation threshold[48]. In addition, our experimental finding of a loss of correlation between band intensity and Fermi-contact constant is reproduced by theory[49].

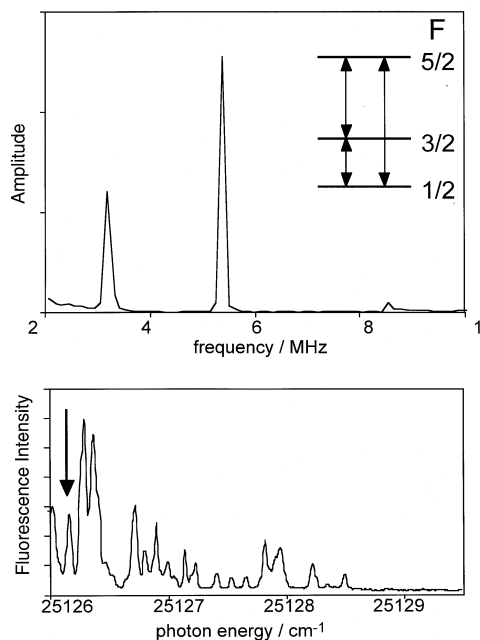


**Figure 5.** Upper panel: Hyperfine quantum beat spectrum for a  $\text{NO}_2$   $J=3/2$  eigenstate near  $D_0$ . The position of this eigenstate is marked by an arrow in the laser induced fluorescence spectrum shown in the lower panel.

We subsequently conducted Zeeman QBS studies of the threshold region[55]. As described above, one hypothesis for the level density anomaly near  $D_0$  involves mixing with repulsive states that are weakly attractive at long-range[43,44,46]. We anticipated that the low-field Landé  $g_F$ -factors would provide valuable information, as six of the ten repulsive states correlating to the  $\text{NO}(^2\Pi) + \text{O}(^3\text{P})$  asymptote are quartet states[56], and calculations predict that at least one of the quartet states has a shallow well at long range[56]. We measured the sign and magnitude of the Landé  $g_F$ -factors for around 20% of the  $J=3/2$  eigenstates within  $15 \text{ cm}^{-1}$  of  $D_0$  using Zeeman polarization QBS[55], observing very small and in some cases, negative, Landé  $g_F$ -factors. This is caused by spin-orbit interactions that mix  $J=3/2$  levels of different  $N, K$  and lead to a breakdown of those quantum numbers. We find that the average Landé factors near  $D_0$  are in good agreement with those predicted on the basis of complete rovibronic mixing[55], and our findings do not show evidence for the participation of quartet states near  $D_0$ .

## B. Probing coupling states using hyperfine and Zeeman spectroscopy: OH/OD

Our work on  $\text{NO}_2$  led us to search for a prototypical system where the spectroscopic manifestations of interactions with repulsive states of higher multiplicity could be characterized. Such a system is  $\text{OH}(\text{OD})$ , where at low energies in the  $A^2\Sigma^+$  state, predissociation via the repulsive  $4\Sigma^-$  state has been implicated both by experiment[57-61] and theory[62-64]. A typical Zeeman polarization quantum beat spectrum for OD is shown in Fig. 6 [65]. The  $A^2\Sigma^+$  state Zeeman interaction is dominated by the isotropic

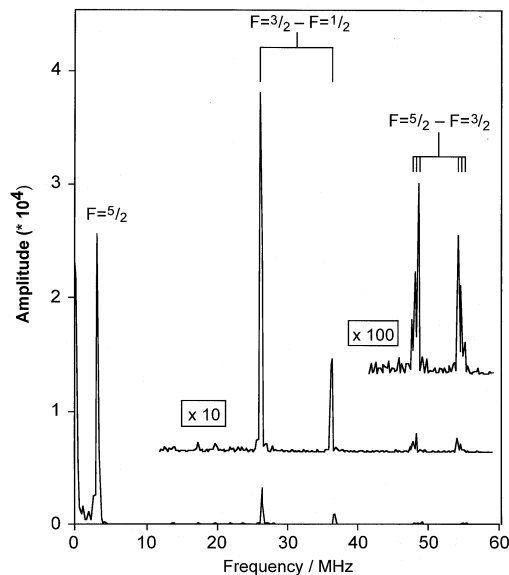


**Figure 6.** Zeeman quantum beat spectrum of the  $R_{21}(1)$  transition in the  $v' = 1 \leftarrow v'' = 0$  band of OD at a field strength of 2.72 G.

electron spin interaction (represented by  $g_s$ ), with small contributions from orbital ( $g_\ell$ ) and rotational ( $g_r$ ) components [12]. In contrast to an earlier report[66], we find  $g_\ell$  and  $g_r$  values for the  $v'=0$  level in the  $\tilde{A}^2\Sigma^+$  state of OD that are consistent with coupling to the ground  $^2\Pi$  state [12]. For example, when fitting the  $v'=0$  data for OH and OD simultaneously using the isotopic correction for  $g_r$ , we find  $g_\ell = -0.007(7)$ , in good agreement with that expected from the measured spin-rotation constants[67] using Curl's relationship[68]. However, at higher energies in the  $\tilde{A}^2\Sigma^+$  state we find, for both OD and OH, that  $g_\ell$  changes sign near the energetic threshold of the  $O(^3P) + H[D](^2S)$  channel [65]. These results cannot be explained within a two-state model involving the ground  $^2\Pi$  state, and our analysis shows that the most probable explanation is interaction with the higher lying  $1^4\Pi$  state[65], which dominates the predissociation at higher energies[57-64].

Our QBS measurements for OD also resolved intermanifold beats [i.e., between different hyperfine components (Fig. 6)] that allowed us to examine the vibrational state dependence of the hyperfine interaction for  $v'=0-3$  [65]. Our results are in good agreement with previous measurements for  $v'=0$  and 1 [66,69-71], and show an increase in the Fermi-contact constant ( $b_F = b + c/3$ ) with increasing  $v'$ , from 118.46(7) MHz for  $v'=0$  to 121.62(15) MHz for  $v'=3$ . The dipole-dipole constant ( $c$ ) decreases with increasing  $v'$ , from 24.85(17) MHz for  $v'=0$  to 21.40(39) MHz for  $v'=3$ , while the small quadrupolar coupling constant ( $eqQ$ ) changes little, from 0.29(5) MHz for  $v'=0$  to 0.31(13) MHz for  $v'=3$ . As the O-D bond stretches, the Fermi-contact interaction is expected to increase, since in the separated atom limit the unpaired electron orbital is a (1s) orbital. The magnitude of the dipole-dipole term ( $c$ ) results primarily from the interaction of the deuteron with the oxygen unpaired spin density, and our results are consistent with the expected  $r^{-3}$  dependence [65]. Calculations for OD( $\tilde{A}^2\Sigma^+$ ;  $v'=0,1$ ) correctly predict the direction of these trends and are within a few percent of the experimental values[72].

### C. Vibrational mode selectivity in hyperfine interactions: HCF

Our studies of the vibrational state dependence of hyperfine interactions were recently extended to a polyatomic molecule, the prototypical singlet carbene HCF, where the vibrational mode dependence of the  $^{19}\text{F}$  and  $^1\text{H}$  hyperfine interaction has been examined in the  $\tilde{A}^1A''$  state[73]. Our measurement of  $C_{aa}$  ( $^{19}\text{F}$ ) for the (0,0,0) level of  $-8.034(87)$  MHz using QBS is in good agreement with the measurement of Hirota and co-workers [ $-7.71(20)$  MHz], who used inter-modulated fluorescence[74]. The  $^{19}\text{F}$  constants increase significantly in magnitude with increasing energy, reflecting in part the energy dependence of the  $A$  rotational constant, which increases dramatically as the barrier to linearity is approached[75,76]. Neglecting small terms arising from closed shell electrons and other nuclei, the nuclear spin/overall rotation constant  $C_{aa}$  can be written as[73,74,77]:

$$C_{aa}(v') = -4A_{\text{eff}} \sum_{v''} \frac{a_{v'v''} \langle \tilde{A}, v' | L_a | \tilde{X}, v'' \rangle^2}{E_{v'} - E_{v''}}, \quad (4)$$

where:  $A_{\text{eff}}$  is the a-axis rotational constant,  $a$  is the nuclear spin/electron orbital coupling constant,  $v$  is a generic vibrational state label,  $L_a$  is the orbital angular momentum operator, and the summation runs over all levels coupled to the state in question.

Consistent with equation (4), we observe a linear dependence of  $C_{aa}({}^{19}\text{F})$  on  $A$  constant for unperturbed states[72]. However, data for the  $(0,n,0)$  and  $(0,n,1)$  sets of vibrational levels falls, respectively, on two *different* lines, revealing an increase in the  ${}^{19}\text{F}$  hyperfine interaction for levels containing C–F stretching excitation. For example,  $C_{aa}({}^{19}\text{F})$  increases by a factor of  $\sim 1.4$  for  $(0,3,1)$  compared to  $(0,3,0)$  and a factor of  $\sim 2.6$  for  $(0,2,1)$  vs.  $(0,2,0)$ . We expect the summation over coupled levels in equation (4) to be similar for unperturbed levels containing equal quanta of bend, as the dominant terms in the sum will involve ground state bending levels. We thus ascribe the observed trend to an increase in the  $a$  constant upon excitation of the C-F stretch, which can be explained in terms of a decrease in back-donation of electron density to the C  $2p_\pi$  orbitals[73].

#### D. Hyperfine interactions as a probe of singlet-triplet interactions in a prototypical carbene: HCF

The utility of QBS for probing singlet-triplet interactions in closed shell systems has been amply demonstrated in the extensive studies of Huber and co-workers[3,5,6,32]. Our studies of HCF have demonstrated that the hyperfine interaction as measured via polarization QBS provides a very sensitive means of discriminating *between* singlet-singlet and singlet-triplet perturbations. To illustrate, we show in the upper panel of Figure 7 experimental and simulated fluorescence excitation spectrum of the

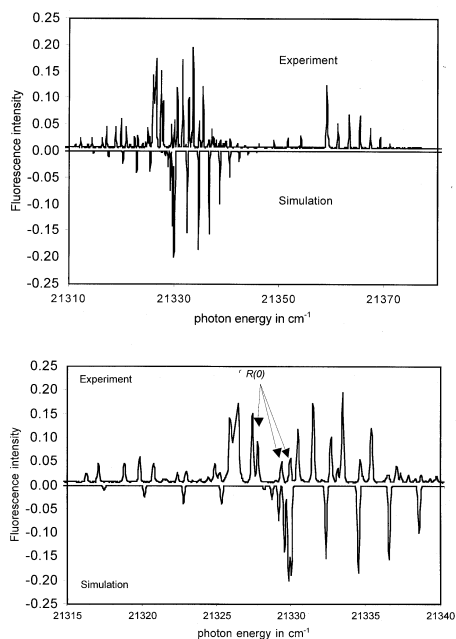


**Figure 7.** Upper panel: experimental and simulated fluorescence excitation spectrum of the  $K_a'=1 \leftarrow K_a''=0$  sub-band of  $(0,4,0)$  level in the  $\tilde{A}^1A''$  state of HCF. Lower panel; Expanded view of the heavily perturbed lower energy sub-band, where the three  ${}^rR(0)$  lines are identified.

$K_a'=1 \leftarrow K_a''=0$  sub-band of (0,4,0). Two sub-bands are clearly observed, split by  $\sim 40$   $\text{cm}^{-1}$ , which we suggest is due to the strong Renner-Teller interaction that couples the  $\tilde{A}^1A''$  state with background  $\tilde{X}^1A'$  levels. Interestingly, while the higher energy sub-band is completely free of rotational perturbations, the lower energy sub-band is severely rotationally perturbed, with the  ${}^rR(0)$  line split into three lines as confirmed by analysis of combination differences. The three  ${}^rR(0)$  lines are identified in the expanded version of the spectrum shown in the lower panel of Figure 7.

In the upper panel of Figure 8 is shown the polarization quantum beat spectrum of the  ${}^rR(0)$  line of the higher energy sub-band. Consistent with our hypothesis, we obtain hyperfine constants that are among the smallest observed (compare, e.g., Figure 8 and Figure 3), which is understood by considering that the constants for  $\tilde{A}^1A''$  and  $\tilde{X}^1A'$  are of similar magnitude but *opposite* sign [74]. Moreover, the Zeeman tuning of this state was too small to measure under our conditions, which also is consistent with mixed  $\tilde{A}^1A''$  and  $\tilde{X}^1A'$  states [74]. Contrast this spectrum with that of the first  ${}^rR(0)$  line of the lower energy sub-band, shown in the lower panel of Figure 8. This level displays the

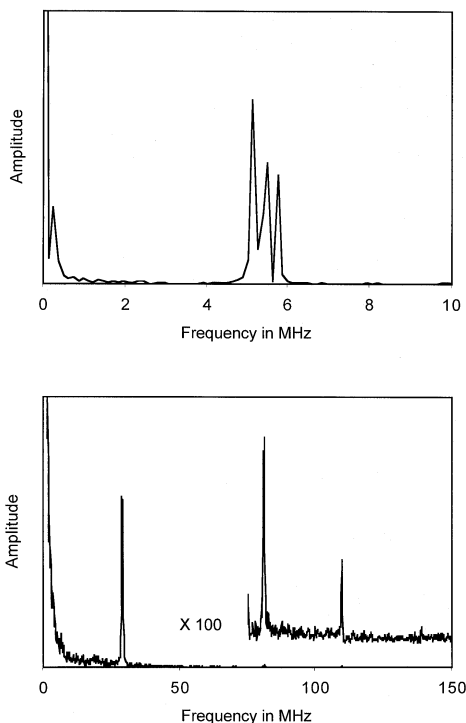


**Figure 8.** Upper panel: Polarization quantum beat spectrum of the  ${}^rR(0)$  line of the higher energy  $K_a'=1 \leftarrow K_a''=0$  sub-band of (0,4,0) level in the  $\tilde{A}^1A''$  state of HCF. Lower panel; Polarization quantum beat spectrum of the first  ${}^rR(0)$  line of the lower energy  $K_a'=1 \leftarrow K_a''=0$  sub-band of (0,4,0)

largest hyperfine splittings observed, and a very large Zeeman effect ( $g_{aa} \sim 0.89$ ), consistent with coupling to the levels of the  $\tilde{a}^3A''$  state.

We combined Zeeman and zero-field hyperfine QBS measurements of triplet-perturbed levels to gain insight into the  $\tilde{a}^3A''$  state properties. For example, taking the pure triplet  $g$ -factor as 2, we infer that the first  ${}^1R(0)$  component of the lower energy sub-band has  $\sim 45\%$  triplet character. To estimate the triplet hyperfine parameters, we conducted preliminary calculations at the QCISD/6-311+G(2df,p) level on the RCCSD(T)/cc-pVQZ optimized triplet state geometry[78], which yield isotropic Fermi-contact constants of 290.43 MHz ( ${}^{19}\text{F}$ ) and 37.6 MHz ( ${}^1\text{H}$ ). Using this result, we predict quantum beat frequencies (in MHz) for the first  ${}^1R(0)$  component of: 11.3 ( $F = 2 \leftrightarrow F = 1$ ), 88.1 ( $F = 2 \leftrightarrow F' = 1$ ), 99.4 ( $F = 1 \leftrightarrow F' = 1$ ), and 110.7 ( $F = 2 \leftrightarrow F = 0$ ), in qualitative agreement with the observed values (Fig. 8). The analysis of these spectra is ongoing, with the goal of glean new information regarding the triplet state properties.

## V. Summary and conclusions

Coherent laser techniques are widely used in molecular spectroscopy and dynamics, and hold much promise for the detailed study of transient molecules and free radicals. We have illustrated the utility of these methods through examples of the application of polarization quantum beat spectroscopy to examine hyperfine structure and Zeeman effects in small transient molecules and free radicals. The studies presented have highlighted the capabilities of coherent spectroscopy as a detailed probe of electronic structure and dynamics. In the future, we anticipate a much broader application of coherent methods to transient molecules.

## Acknowledgements

The authors gratefully acknowledge the donors of the Petroleum Research Fund of the American Chemical Society and the National Science Foundation (under grant CHE-9702803) for partial support of this work.

## References

1. Ernst, R. N., Bodenhausen, G., and Wokaun, A. 1987, Principles of Nuclear Magnetic Resonance in One and Two Dimensions, Clarendon Press, Oxford.
2. Zewail, A. H. 1995, Femtosecond Chemistry, J. Manz and L. Wöste (Eds.), VCH, Weinheim.
3. See, e.g., 1998, Nonlinear Spectroscopy for Molecular Structure Determination, R. W. Field, E. Hirota, J. P. Maier, and S. Tsuchiya (Eds.), Blackwell Science, Oxford.
4. Wang, Z.-G. and Xia, H.-R. 1991, Molecular and Laser Spectroscopy (Springer Series in Chemical Physics; Vol. 50), Springer Verlag, Berlin.
5. Bitto, H. and Huber, J. R. 1990, Opt. Commun. 80, 184.
6. Carter, R. T. and Huber, J. R. 2000, Chem. Soc. Rev. 29, 305.
7. Haroche, S. 1976, High Resolution Laser Spectroscopy, K. Shimoda (Ed.), Springer Verlag, Berlin, Ch. 7.
8. Schmitt, M., Siebert, T., and Kiefer, W. 2003, Indian J. Phys. B, 77, 49.
9. Dantus, M. 2001, Ann. Rev. Phys. Chem., 52, 639.
10. Vasilenko, L. S. and Rubtsova, N. N. 1997, Laser Physics, 7, 1021.
11. Hirota, E. 1985, High-Resolution Spectroscopy of Transient Molecules (Springer Series in Chemical Physics; Vol. 40), Springer Verlag, Berlin.

12. Raab, F., Bergeman, T., Lieberman, D., and Metcalf, H. 1981, *Phys. Rev. A*, 24, 3120.
13. Brucat, P. J. and Zare, R. N. 1983, *J. Chem. Phys.*, 78, 100.
14. Attal, B., Débarre, D., Müller-Dethlefs, K., and Taran, J.P.E. 1983, *Rev. Phys. Appl.*, 18, 39.
15. Farrow, R. L. and Rakestraw, D. J. 1992, *Science*, 257, 1894.
16. Nyholm, K., Maier, R., Aminoff, C. G., and Kaivola, M. 1993, *Appl. Optics*, 32, 919.
17. Povey, I. M., Carter, R. T., Bitto, H. and Huber, J. R. 1996, *Chem. Phys. Lett.* 248, 470.
18. Brock, L. R. and Rohlfing, E. A. 1997, *J. Chem. Phys.*, 106, 10048.
19. Harper, W. W., Waddell, K., and Clouthier, D. J. 1997, *J. Chem. Phys.*, 107, 8829.
20. Dreier, T. and Ewart, P. 2002, *Applied Combustion Diagnostics*, K. Kohse-Höinghaus and J. B. Jeffries (Eds.), Taylor & Francis, New York, pp. 69–97.
21. Tan, X. Q., Wright, T. G., and Miller, T. A. 1995, *Jet Spectroscopy and Molecular Dynamics*, J. M. Hollas and D. Phillips (Eds.), Blackie, London, pp. 74-117.
22. Tang, Y. and Reid, S. A. 1998, *Chem. Phys. Lett.*, 292, 691.
23. Tang, Y., Schmidt, J. P., and Reid, S. A. 1999, *J. Chem. Phys.*, 110, 5734.
24. Hung, W.-C., Huang, M.-L., Lee, Y.-C., and Lee, Y.-P. 1995, *J. Chem. Phys.*, 105, 9941.
25. Chaiken, J. Benson, T., Gurnick, M., and McDonald, J. D. 1979, *Chem. Phys. Lett.*, 61, 195.
26. Chaiken, J., Gurnick, M., and McDonald, J. D. 1981, *J. Chem. Phys.* 74, 106.
27. Mühlbach, J., Dubs, M., Bitto, H., and Huber, J. R. 1984, *Chem. Phys. Lett.*, 111, 288.
28. Bitto, H., Stafast, H., Russegger, P., and Huber, J. R. 1984, *Chem. Phys.*, 84, 249.
29. Bitto, H., Willmott, P. R., and Huber, J. R. 1991, *J. Chem. Phys.*, 95, 4765.
30. Blum, K. 1996, *Density Matrix Theory and Applications*, Plenum, New York.
31. Dubs, M., Mühlbach, J., and Huber, J. R. 1986, *J. Chem. Phys.*, 85, 1288.
32. Hack, E., Bitto, H., and Huber, J. R. 1991 *Z. Phys. D: At., Mol. Clusters*, 18, 33.
33. Xin, J., Fan, H., Ionescu, I., Annesley, C., and Reid, S. A. 2003, *J. Mol. Spectrosc.*, 219, 37.
34. Delon, A. and Jost, R. 1991, *J. Chem. Phys.*, 95, 5686.
35. Delon, A., Lombardi, M., and Jost, R. 1991, *J. Chem. Phys.* 95, 5701.
36. Georges, R., Delon, A., and Jost, R. 1995, *J. Chem. Phys.*, 103, 1732.
37. Miyawaki, J., Yamanouchi, K. and Tsuchiya, S. 1993, *J. Chem. Phys.*, 99, 254.
38. Miyawaki, J., Yamanouchi, K. and Tsuchiya, S. 1994, *J. Chem. Phys.*, 101, 4505.
39. Ionov, S. I., Davis, H. F., Mikhaylichenko, K., Valachovic, L., Beaudet, R. A. and Wittig, C. 1994, *J. Chem. Phys.*, 101, 4809.
40. Abel, B., Hamann, H. H., and Lange, N., 1995, *Faraday Discuss.*, 102, 147.
41. Jost, R., Nygård, J., Pasinski, A. and Delon, A. 1996, *J. Chem. Phys.*, 105, 1287.
42. Jost, R., Nygård, J., Pasinski, A. and Delon, A. 1997, *Phys. Rev. Lett.* 78, 3093.
43. Romanini, D., Kachanov, A. A. and Stoeckel, F. 1997, *Chem. Phys. Lett.*, 270, 538.
44. Delon, A., Heilliette, S. and Jost, R. 1998, *Chem. Phys.*, 238, 465.
45. Delon, A. Reiche, F., Abel, B., Grebenshchikov, S. Y. and Schinke, R. 2000, *J. Phys. Chem A* 104, 10374.
46. Heilliette, S., Delon, A., Dupre, P., and Jost, R. 2001, *Phys. Chem. Chem. Phys.*, 3, 2268.
47. Bezel, I., Stolyarov, D., and Wittig, C. 1999, *J. Phys. Chem. A* 103, 10268.
48. Xin, J. and Reid, S. A., 2000, *J. Chem. Phys.* 112, 10067.
49. Xin, J. Reid, S. A., Santoro, F. and Petrongolo, C. 2001, *J. Chem. Phys.*, 115, 8868.
50. Vedder, H. J., Persch, G. and Foth, H.-J. 1985, *Chem. Phys. Lett.*, 114, 125.
51. Persch, G., Vedder, H. J. and Demtröder, W. 1986, *Chem. Phys.*, 105, 471.
52. Persch, G., Vedder, H. J., and Demtröder, W. 1987, *J. Mol. Spectrosc.*, 123, 356.
53. Biesheuvel, C. A., ter Steege, D. H. A., Bulthuis, J., Janssen, M. H. M., Snijders, J. G., and Stolte, S. 1997, *Chem. Phys. Lett.*, 269, 515.
54. Biesheuvel, C. A., Bulthuis, J., Janssen, M. H. M., Snijders, J. G., and Stolte, S. 1998, *J. Chem. Phys.*, 109, 9701.
55. Xin, J. and Reid, S. A. 2002, *J. Chem. Phys.*, 116, 515.
56. Katagiri, H. and Kato, S. 1993, *J. Chem. Phys.*, 99, 8805.

57. German, K. R. 1975, *J. Chem. Phys.*, 63, 5255.
58. Bergeman, T, Erman, P, Haratym, Z., and Larsson, M. 1981, *Phys. Scr.*, 23, 45.
59. Spaanjaars, J. J. L., ter Meulen, J. J., and Meijer, G. 1997, *J. Chem. Phys.*, 107, 2242.
60. Gray, J. A. and Farrow, R. L. 1991, *J. Chem. Phys.*, 95, 7054.
61. Heard, D. E., Crosley, D. R., Jeffries, J. B., Smith, G. P., and Hirano, A. 1992, *J. Chem. Phys.*, 96, 4366.
62. Yarkony, D. R. 1992, *J. Chem. Phys.*, 97, 1838.
63. Parlant, G. and Yarkony, D. R. 1999, *J. Chem. Phys.*, 110, 363.
64. Lee, S. 1996, *J. Chem. Phys.*, 104, 7914.
65. Xin, J., Ionescu, I., Kuffel, D. and Reid, S. A. 2003, *Chem. Phys.*, 291, 61.
66. Carter, R. T., Povey, I. M., Bitto, H. and Huber, J. R. 1996, *J. Chem. Phys.*, 104, 5365.
67. Coxon, J. A. 1975, *J. Mol. Spectrosc.*, 58, 1.
68. Curl, R. F. 1965, *Mol. Phys.*, 5, 585.
69. German, K. R., Bergeman, T. H., Weinstock, E. M. and Zare, R. N. 1973, *J. Chem. Phys.*, 58, 4304.
70. Weinstock, E. M. and Zare, R. N. 1973, *J. Chem. Phys.*, 58, 4319.
71. German, K. R. 1976, *J. Chem. Phys.*, 64, 4192.
72. Green, S. 1973, *J. Chem. Phys.*, 58, 4327.
73. Ionescu, I., Fan, H., Annesley, C., Xin, J., and Reid, S. A. 2004, *J. Chem. Phys.* (in press; publication date 1/15/04).
74. Suzuki, T. and Hirota, E. 1986, *J. Chem. Phys.*, 85, 5541.
75. Schmidt, T. W., Bacskay, G. B., and Kable, S. H. 1999, *J. Chem. Phys.*, 110, 11277.
76. Fan, H., Ionescu, I., Annesley, C., and Reid, S. A. 2003, *Chem. Phys. Lett.*, 378, 548.
77. Townes, C. H. and Schawlow, A. L. 1955, *Microwave Spectroscopy*, McGraw-Hill, New York, Ch. 8.
78. Schmidt, T. W., Bacskay, G. B., and Kable, S. H. 1998, *Chem. Phys. Lett.*, 292, 80.